OKSU-SBW-4

DTIE MICROCARD ISSUANCE DATE

9/12

1963

D-3

SCDC-3284

G. Bowen

TID-19116

REPORT SBW-4

COMPUTATION CURVES FOR AXI-SYMMETRIC BASE PRESSURE ANALYSIS

By

GLEN W. ZUMWALT and HOMER H. TANG

Prepared for
SANDIA CORPORATION
ORGANIZATION NO. 7131
(Purchase Order 82-4326)

School of Mechanical Engineering
Oklahoma State University
Stillwater, Oklahoma
March, 1963

PREFACE

A research contract between Sandia Corporation and Oklahoma State University calls for analysis of base pressures under the highly transient conditions which occur when a supersonic missile flys through a blast wave. During the transient phase, the computation method requires solutions of the axi-symmetric base pressure to be found for successive time increments while the jet-mixing surfaces are acting as ejectors and the free stream conditions vary with time. Due to the complexity of even steady-state solutions of axi-symmetric base pressures, it has become necessary to provide as much of the calculations as possible in graphical form. The curves presented here are applicable to turbulent, compressible jet mixing, where the total temperature is constant across the mixing region, and the flow streamlines converge conically. The principal parameter obtainable from these curves is the dimensionless velocity of the streamline which divides the free stream flow mass from the flow mass entrained from the "dead-air" near the base of the body.

LIST OF SYMBOLS

B	Dimensionless group defined in Equation 2, page 2
$C = \frac{u}{u_{max}}$,	Crocco number = $\left[\frac{M^2}{\frac{2}{k-1} + M^2}\right]^{\frac{1}{2}}$
d	Diameter of sting
D	Diameter of body
$f(\ )$	Function of some variables
I_1	Integral defined on p. 2
I_2	Integral defined on p. 2
J_1	Integral defined on p. 2
J_2	Integral defined on p. 2
K	Ratio of specific heats
M	Mach number
p	Absolute pressure
R	Radius of body
$\bar{R}$	Radius of the "sting," a cylindrical body extending axially from the base.
$\mathbb{R}$	A reference streamline near but outside the mixing region
V	Velocity in x or X direction
x, y	Coordinates of the intrinsic coordinate system
X, Y	Coordinates of the reference coordinate system
σ	Similarity parameter of the homogeneous coordinate y/x (Also called the tree jet parameter)

$\eta = \sigma\, y/x$, Dimensionless coordinate

Θ	Streamline angle
$\varphi = \frac{u}{u_a}$	Dimensionless velocity

Subscripts

1, 2, 3, 4	Refer to conditions at cross sections indicated in Fig. 1.
a	Refers to conditions of the flow in the isentropic stream adjacent to the dissipative regions
b	Refers to the conditions at the base of the sudden expansion
d	Refers to the streamline whose kinetic energy is just sufficient to enter the recompression region.
j	Refers to conditions along the jet boundary streamline.
m	Refers to coordinate shift in the mixing theory due to the momentum integral.
o	Stagnation conditions
$\mathbb{R}$	Refers to conditions along the $\mathbb{R}$ streamline

TABLE OF CONTENTS

INTRODUCTION

The conical pressure rise theory for separated flows, which was developed by the first author in Ref. 1, has been adapted for calculating axi-symmetric body base pressure in this technical note. The computation complexity of the theory has been reduced by the provision of auxiliary curves, plotted as Figures 2 to 21. Furthermore, several typical solutions for steady flow have been calculated for M = 1.5, 2.0, 3.0, 4, and 5 in order to check the theory with some published experimental results.

All axi-symmetric flow field theories fail for flow converging on the centerline, and the axi-symmetric base pressure theory is no exception. The mathematical difficulties for the flow field of an axi-symmetric body with an empty base have been conveniently avoided by using a "sting" which is concentric with the body (see Fig. 1). Thus, the conical pressure rise theory has been established for this flow model. Fortunately, the theory predicts that base pressure will be almost a constant value when $d/D < 0.4$, and this agrees well with experimental data (Ref. 2). Hence, the theory which assumes a small d/D ratio sting on the base is sufficiently accurate to predict base pressure for a no-sting axi-symmetric body.

I. RESUME OF CONICAL PRESSURE RISE THEORY

In Ref. 1, the author wrote the momentum equation in the axial direction with some geometrical and reference coordinate transformations. This was solved simultaneously with the combined viscid and inviscid continuity equations between the separation corner cross-section, section 2, and a downstream flow cross-section, 3 (see Fig. 1), for the mass passing along the annular stream tube bounded by streamlines j and a distant streamline ($\eta_{IR} = 3$). He obtained the governing equation as follows:

$$(B-3)^2 + 2(1-C_{3a}^2)\left[I_1\Big|_{-\infty}^{3} - I_1\Big|_{-\infty}^{\varphi_j} \right]B - 2(1-C_{3a}^2)\left[J_1\Big|_{-\infty}^{3} - J_1\Big|_{-\infty}^{\varphi_j} \right] = \left(\frac{\sigma\bar{R}}{x\cos\theta}\right)_{3a}^2 \qquad \text{Eqn. 1}$$

where

$$B = \frac{J_1\Big|_{-\infty}^{\varphi_j} - \left(1-\frac{C_{3a}}{C_{2a}}\right)J_1\Big|_{-\infty}^{3} - \frac{C_{3a}}{C_{2a}}(J_1-J_2)\Big|_{-\infty}^{3}}{I_1\Big|_{-\infty}^{\varphi_j} - \left(1-\frac{C_{3a}}{C_{2a}}\right)I_1\Big|_{-\infty}^{3} - \frac{C_{3a}}{C_{2a}}(I_1-I_2)\Big|_{-\infty}^{3} + \frac{k-1}{K}\,\frac{3}{C_{2a}C_{3a}}\left(1-\frac{p_2}{p_3}\right)} \qquad \text{Eqn. 2}$$

$$I_1 = \int_{-\infty}^{\eta} \frac{\varphi}{1-C_a^2\varphi^2}\, d\eta \qquad \text{Eqn. 3}$$

$$I_2 = \int_{-\infty}^{\eta} \frac{\varphi\eta}{1-C_a^2\varphi^2}\, d\eta \qquad \text{Eqn. 4}$$

$$J_1 = \int_{-\infty}^{\eta} \frac{\varphi^2}{1-C_a^2\varphi^2}\, d\eta \qquad \text{Eqn. 5}$$

$$J_2 = \int_{-\infty}^{\eta} \frac{\varphi^2\eta}{1-C_a^2\varphi^2}\, d\eta \qquad \text{Eqn. 6}$$

In Equations 1 and 2, the integrals are evaluated at C_{3a}.

It is evident that, for fixed geometry, the integral Equation (1) includes four variables, namely, C_{2a}, C_{3a}, φ_{j3}, and θ_{34}. It might be possible to obtain a direct solution if a proper relationship could be found. The work now being carried on by the second author for his Ph. D. dissertation, expected to be published later this year, may provide some empirical formulations to relate the four variables mutually.

In this note, we simply provide graphs which include the most practical combinations of these four variables to allow a trial and error technique to be applicable. Calculation procedures have also been suggested.

II. CALCULATION PROCEDURES

For a given uniform M_1 flowing steadily near the end of a cylinder, the calculation for the pressure on the base of the cylinder is as follows: Select a typical value of θ_{12}, then locate a proper $\bar{R}/R$ position by the trial and error method below.

A. M_{2a} or C_{2a} can be obtained when M_1 and θ_{12} are given by using Prandtl-Meyer expansion relations locally at the cylinder end.

B. Assume an $\bar{R}/R$ value, then an empirical equation based on conical afterbody characteristic solutions yields M_{3a} or C_{3a} as

$$M_{3a} = \frac{M_{2a}}{e^{0.209(1-\bar{R}/R)}}$$

Hence, for each assumed $\bar{R}/R$ value, M_{3a} can be obtained. Note that $C_{3a}^2 = M_{3a}^2 / 5 + M_{3a}^2$ for air at moderate temperatures.

C. Calculate $\left(\frac{\bar{R}\ \sigma}{x\cos\theta}\right)^2_{3a}$:

1) Let $\theta_{34} = \theta_{12}$ (conical wake assumption)

2) $\sigma \cong 47.1\ C_{3a}^2$ (experimental basis)

3) $$\left(\frac{\bar{R}\ \sigma}{x\cos\theta}\right)^2_{3a} = \left[\frac{\sigma\ \tan\theta_{34}}{\frac{1}{\bar{R}/R} - 1}\right]^2_{3a}$$

D. Values of $\left(\frac{\bar{R}\ \sigma}{x\cos\theta}\right)^2_{3a}$, C_3^2, C_{3a}/C_{2a} will allow one to find φ_j from Figures 2 to 7.

E. Since non-bleed wake prevails for steady flow, $\varphi_d = \varphi_j$, and $C_d \equiv \varphi_d\ C_{3a}$.

F. But also, $$C_d = \left[1 - \frac{1}{\left(\frac{p_4}{p_3}\right)^{0.286}}\right]^{\frac{1}{2}}$$

where p_4/p_3 is the pressure ratio across an oblique shock of a stream flowing with velocity M_{3a} deflected through an angle θ_{34}.

If $\varphi_d\ C_{3a} \neq \left[1 - \frac{1}{\left(\frac{p_4}{p_3}\right)^{0.286}}\right]^{\frac{1}{2}}$, we should repeat from step B.

For convenience, this check can be made instead by using a family of curves of C_{3a} vs φ_d to read θ_{34} values directly from Figure 22. Therefore, after φ_j has been found in step D, then known $\varphi_d (=\varphi_j)$ with the known C_{3a} value allows us to find θ_{34} immediately. If $\theta_{34} \neq \theta_{12}$, then repeat the calculation from step B.

G. With correct $\bar{R}/R$, M_{2a} θ_{12} values, p_b/p_1 at specific position $\bar{R}/R$ can be obtained by the isentropic flow relation as:

$$\frac{p_b}{p_1} = \frac{p_2}{p_1} = \frac{\left.\frac{p_2}{p_{o2}}\right|_{f(M_2)}}{\left.\frac{p_1}{p_{o1}}\right|_{f(M_1)}}$$

The base pressure is now known for a particular $\bar{R}/R$. A curve results similar to Figure 23.

III. CALCULATION RESULTS

The conical pressure rise theory has been used to calculate the steady base pressures for Mach numbers 1.5, 2, 3, 4, and 5. The first three results check well with available experimental data. Results are plotted in Figure 23. The nearly constant value of p_b/p_1 in the region of small $\bar{R}/R$ values is the base pressure for a blunt base at M_1. Fortunately, they result in a simple empirical formula as

$$\frac{p_b}{p_1} = 0.928 - \ln \sqrt{M_1} \qquad \text{Eqn. 7}$$

for $1.2 \leq M_1 \leq 5$. (See Figure 24.)

Evidently this formula cannot be used when $M_1 > 5$. It is suggested to obtain data for high Mach numbers so that an equation can be employed to form another simple relation which is valid in the region of hypersonic flows. Until this is done, an estimated value is shown for this region in Figure 24.

IV. FURTHER APPLICATIONS

With the assistance of Eqn. 7, we can obtain quasi-steady base pressure solutions for a missile base with a head-on passing blast wave by using the moving shock technique which is described in detail in Ref. 3, p. 54. Other non-steady base pressure problems can be treated similarly.

Also, for a base with downstream non-cylindrical body, a solution can be obtained by using the "Equivalent Parallel Flow" technique which has been described in detail in Ref. 4.

REFERENCES

1. Zumwalt, G. W. Analytical and Experimental Study of the Axially Symmetric Supersonic Base Pressure Problem, Ph. D. Dissertation, University of Illinois, 1959.

2. Beheim, M. A. Flow in the Base Region of Axisymmetric and Two-Dimensional Configurations, Lewis Research Center, NASA-TR--R-77, 1960.

3. Zumwalt, G. W. and Tang, H. H. Blast Wave Effect on Missile Base Pressure, Research Report SBW-1 for Sandia Corporation, P. O. 12-3012, Office of Engineering Research, Oklahoma State University, June 1961, pp. 41, 54; Fig. 2.

4. Korst, H. H, Chow, W. L., and Zumwalt, G. W. Research on Transonic and Supersonic Flow of a Real Fluid at Abrupt Increases in Cross Section, ME-TN-392, Engineering Experiment Station, University of Illinois, December, 1959.

5. Chapman, D. R., An Analysis of Base Pressure at Supersonic Velocities and Comparison with Experiments. NACA Report 1051, 1951.

6. Sivier, K. R. and Bogdonoff, S. M., The Effect of Support Interference on the Base Pressure of a Body of Revolution, Report No. 332, Princeton University, October 1955. (AFOSR TN-55-301)

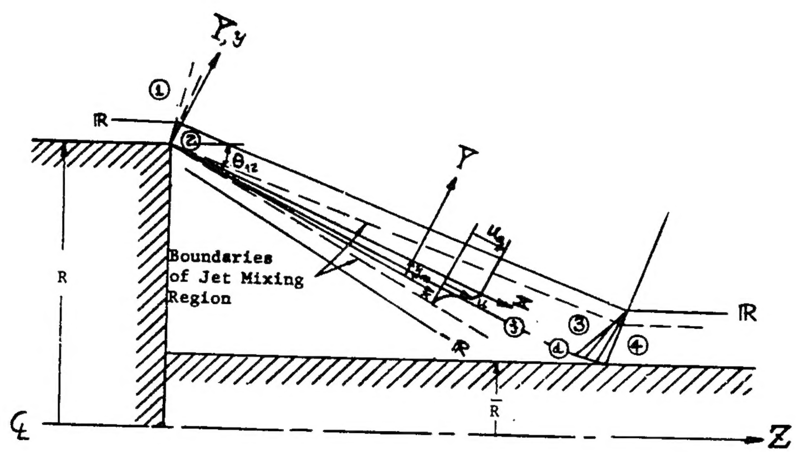

Figure 1. Flow Model For Use in The Analysis of a Free Jet Boundary With Rising Pressure.

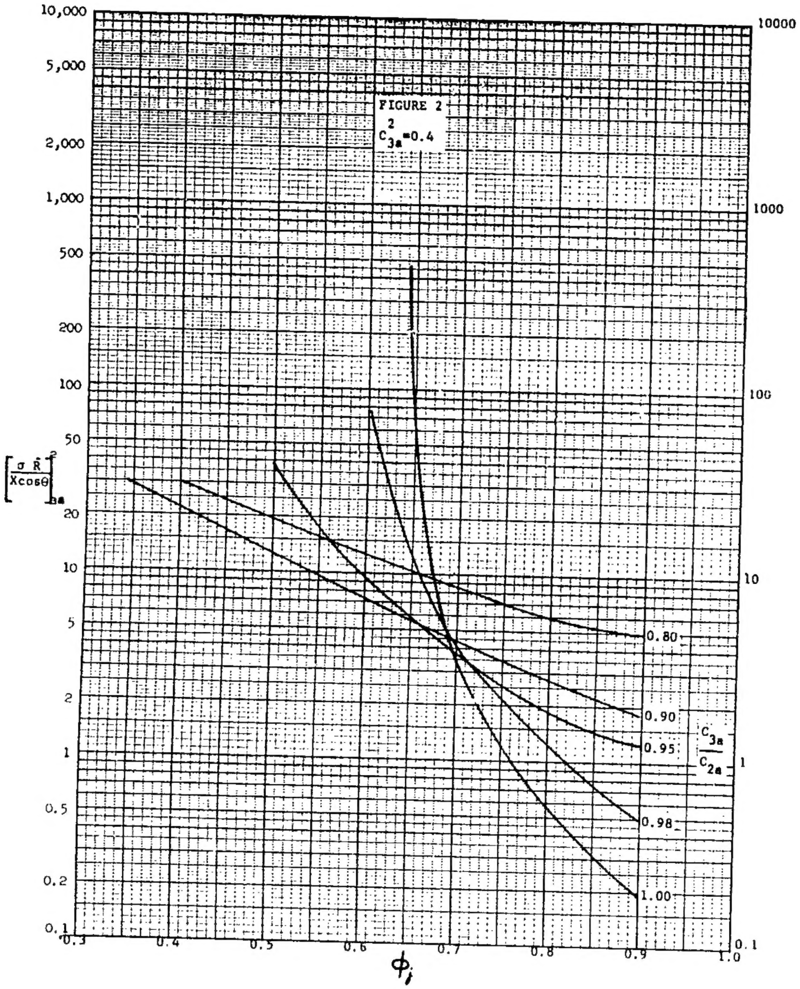
FIGURE 2
$C^2_{3a}=0.4$
$\left[\frac{\sigma \bar{R}}{X\cos\theta}\right]^2_{3a}$
ϕ_i
$\frac{C_{3a}}{C_{2a}}$
0.80
0.90
0.95
0.98
1.00

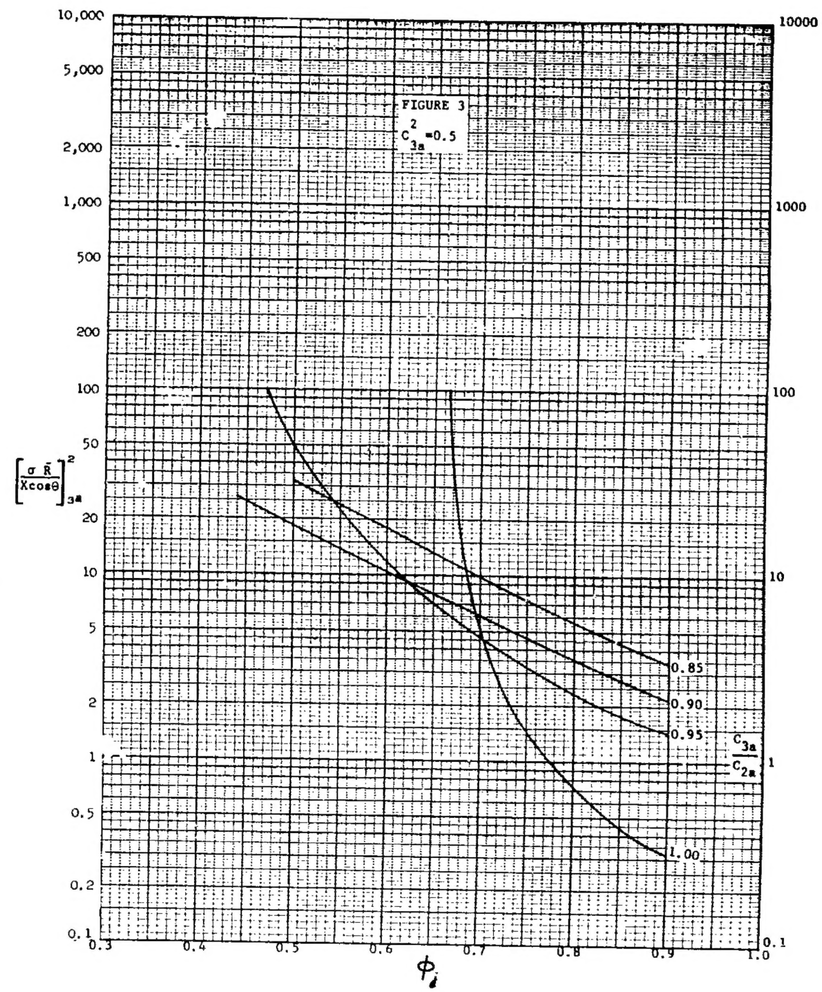
FIGURE 3
$C^2_{3a}=0.5$
$\left[\frac{\sigma \bar{R}}{X\cos\theta}\right]^2_{3a}$
ϕ_i
$\frac{C_{3a}}{C_{2a}}$
0.85
0.90
0.95
1.00

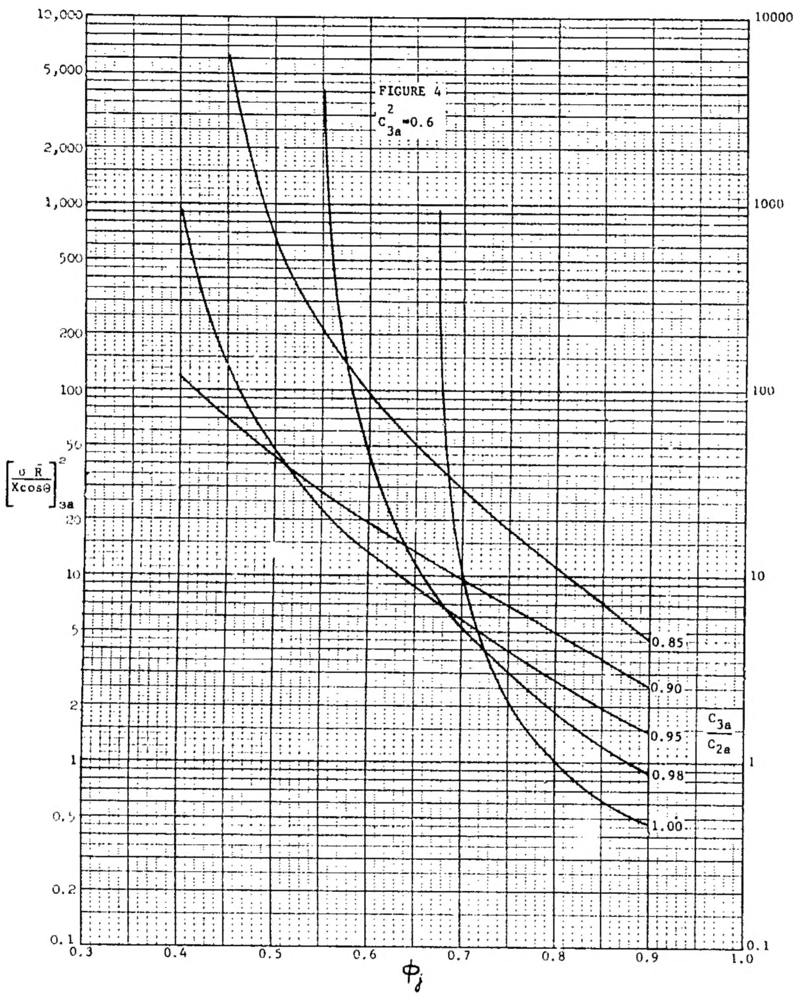
FIGURE 4
$C_{3a}^{2}=0.6$
$\left[\frac{\sigma \bar{R}}{X\cos\theta}\right]^{2}_{3a}$
ϕ_j
$\frac{C_{3a}}{C_{2a}}$
0.85
0.90
0.95
0.98
1.00

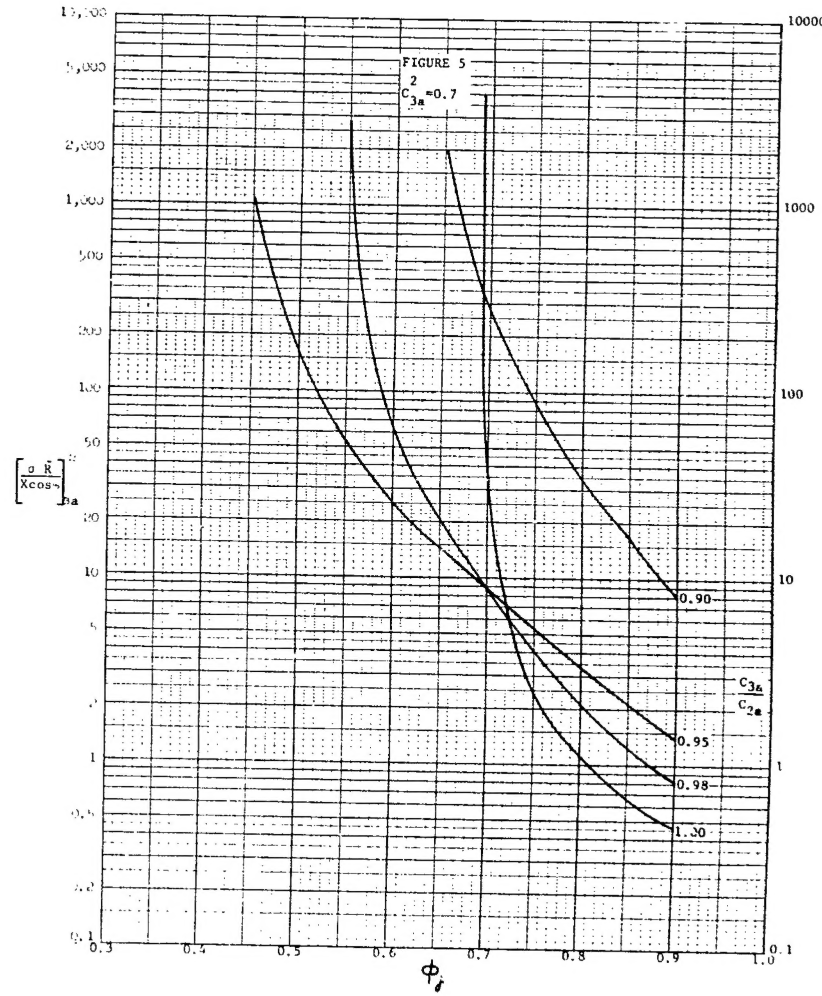
FIGURE 5
$C_{3a}^{2}=0.7$
ϕ_j
$\frac{C_{3a}}{C_{2a}}$
0.90
0.95
0.98

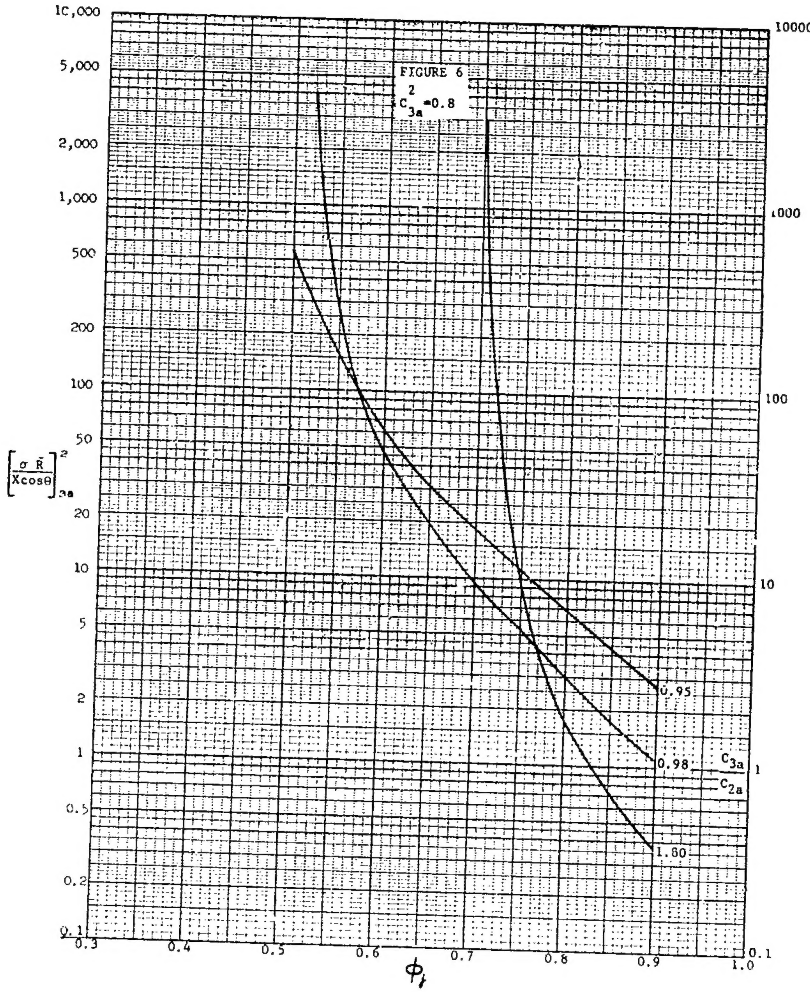

FIGURE 6
$C_{3a}^2 = 0.8$
$\left[\frac{\sigma \bar{R}}{X\cos\theta}\right]^2_{3a}$
10,000
5,000
2,000
1,000
500
200
100
50
20
10
5
2
1
0.5
0.2
0.1
0.3
0.4
0.5
0.6
0.7
0.8
0.9
1.0
ϕ_i
0.95
0.98
1.00
$\frac{C_{3a}}{C_{2a}}$
10000
1000
100
10
1
0.1

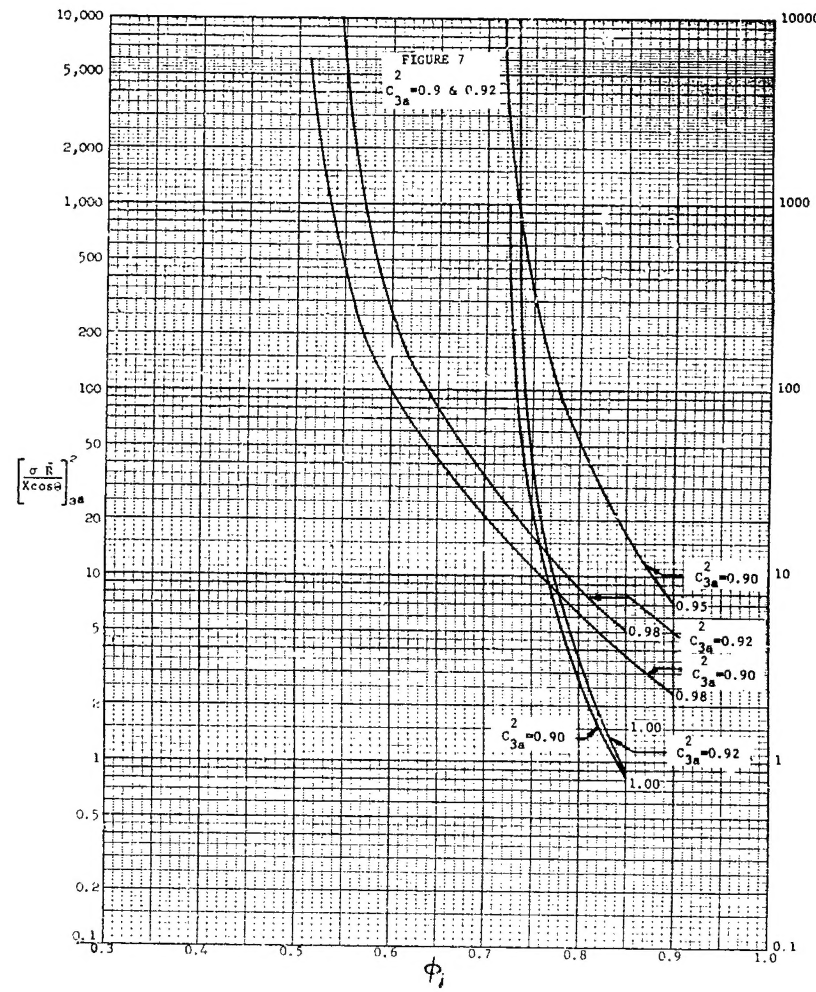

FIGURE 7
$C_{3a}^2 = 0.9$ & 0.92
$\left[\frac{\sigma \bar{R}}{X\cos\theta}\right]^2_{3a}$
10,000
5,000
2,000
1,000
500
200
100
50
20
10
5
1
0.5
0.2
0.1
0.3
0.4
0.5
0.6
0.7
0.8
0.9
1.0
ϕ_i
$C_{3a}^2 = 0.90$
0.95
0.98
$C_{3a}^2 = 0.92$
$C_{3a}^2 = 0.90$
0.98
1.00
$C_{3a}^2 = 0.90$
$C_{3a}^2 = 0.92$
1.00
10000
1000
100
10
1
0.1

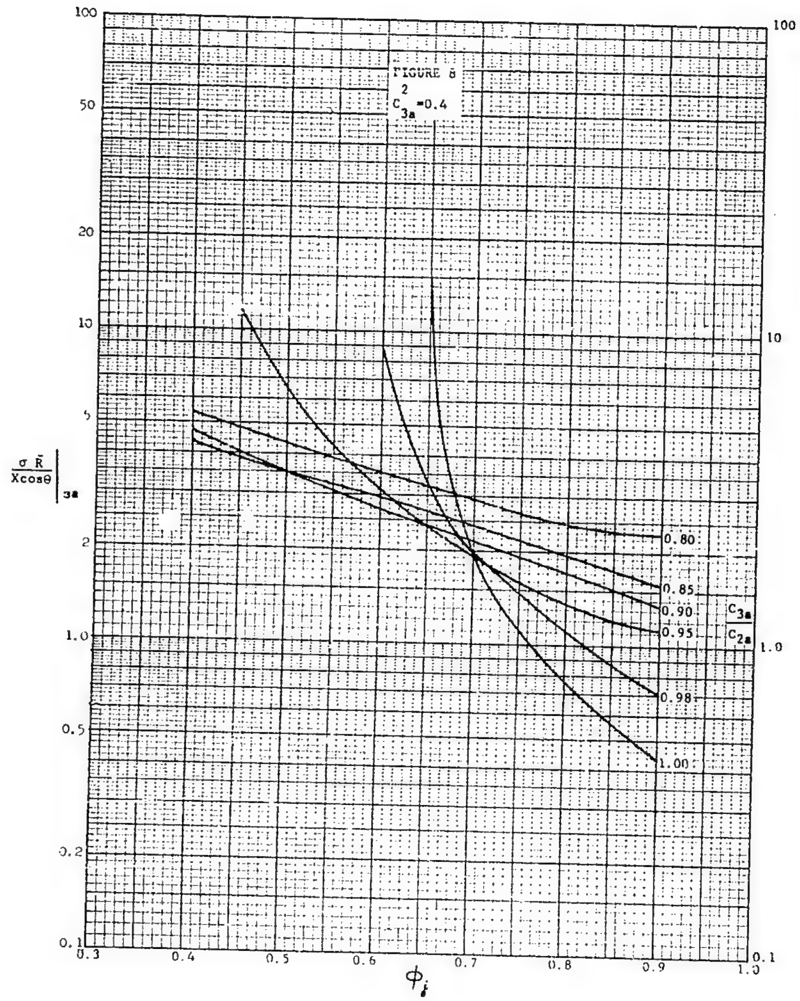
FIGURE 8
$C_{3a}^2 = 0.4$
$\frac{\sigma \bar{R}}{X\cos\theta}\Big|_{3a}$
$\frac{C_{3a}}{C_{2a}}$
0.80
0.85
0.90
0.95
0.98
1.00
ϕ_i
100
50
20
10
5
2
1.0
0.5
0.2
0.1
0.3
0.4
0.5
0.6
0.7
0.8
0.9
1.0

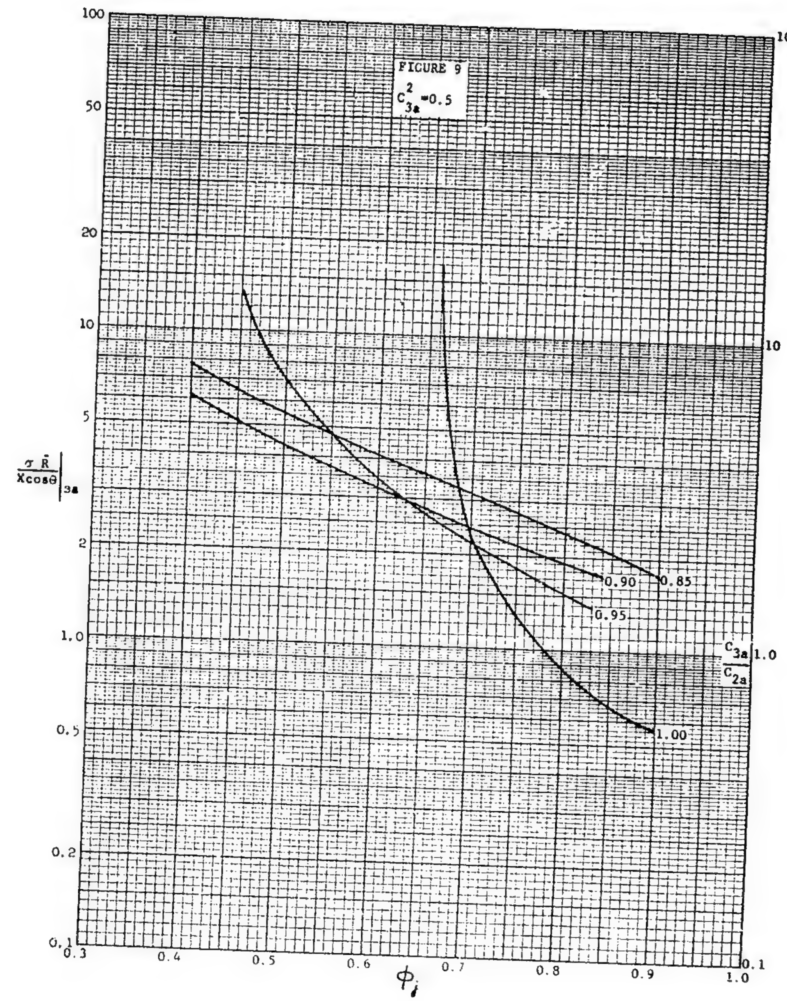
FIGURE 9
$C_{3a}^2 = 0.5$
$\frac{\sigma \bar{R}}{X\cos\theta}\Big|_{3a}$
$\frac{C_{3a}}{C_{2a}}$
0.85
0.90
0.95
1.00
ϕ_i
100
50
20
10
5
2
1.0
0.5
0.2
0.1
0.3
0.4
0.5
0.6
0.7
0.8
0.9
1.0

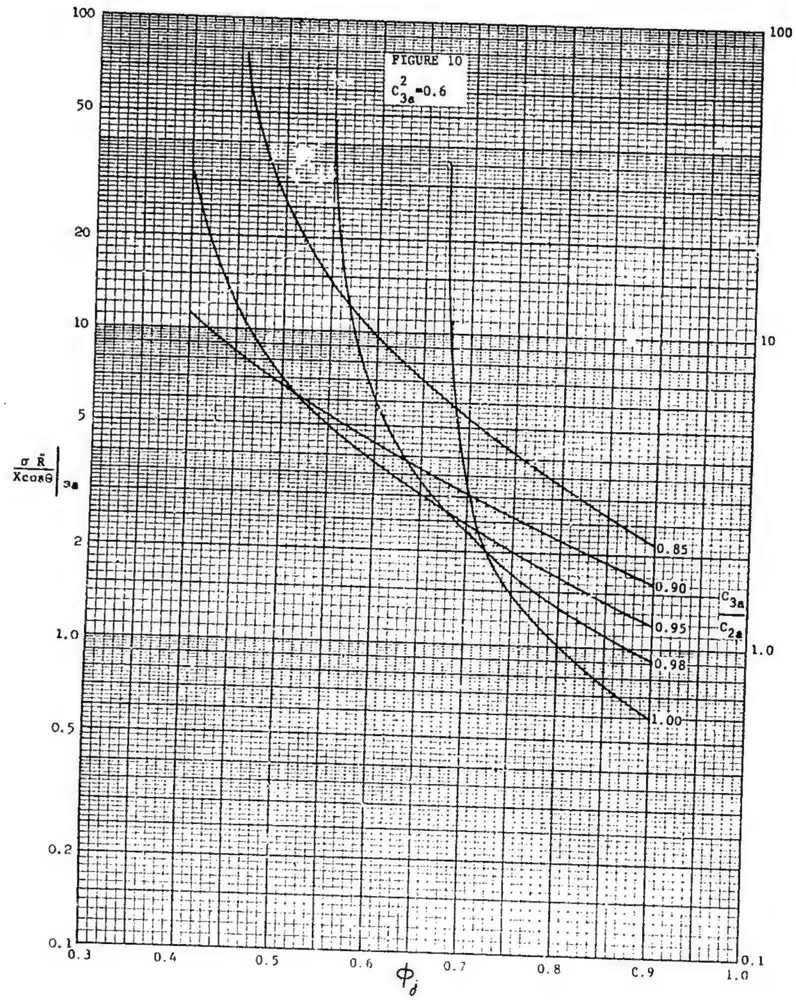

FIGURE 10
$C_{3a}^2 = 0.6$
$\frac{\sigma \bar{R}}{X \cos\theta}\Big|_{3a}$
100
50
20
10
5
2
1.0
0.5
0.2
0.1
0.3
0.4
0.5
0.6
0.7
0.8
0.9
1.0
Φ_j
0.85
0.90
0.95
0.98
1.00
$\frac{C_{3a}}{C_{2a}}$

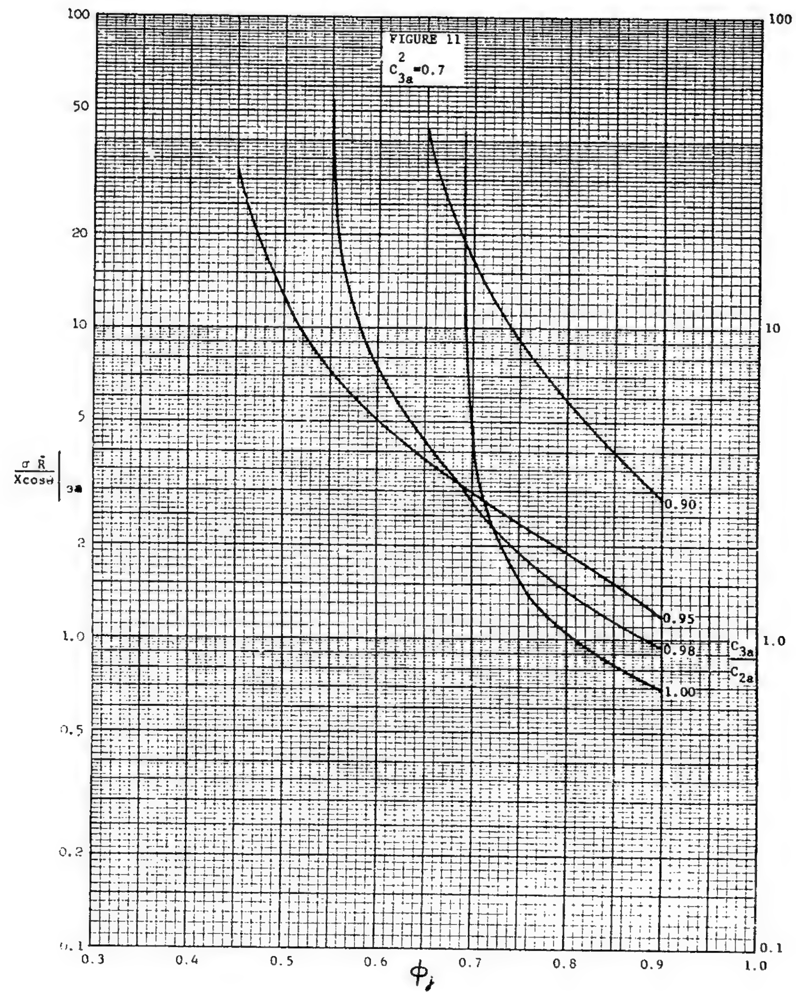

FIGURE 11
$C_{3a}^2 = 0.7$
$\frac{\sigma \bar{R}}{X \cos\theta}\Big|_{3a}$
100
50
20
10
5
2
1.0
0.5
0.2
0.1
0.3
0.4
0.5
0.6
0.7
0.8
0.9
1.0
Φ_j
0.90
0.95
0.98
1.00
$\frac{C_{3a}}{C_{2a}}$

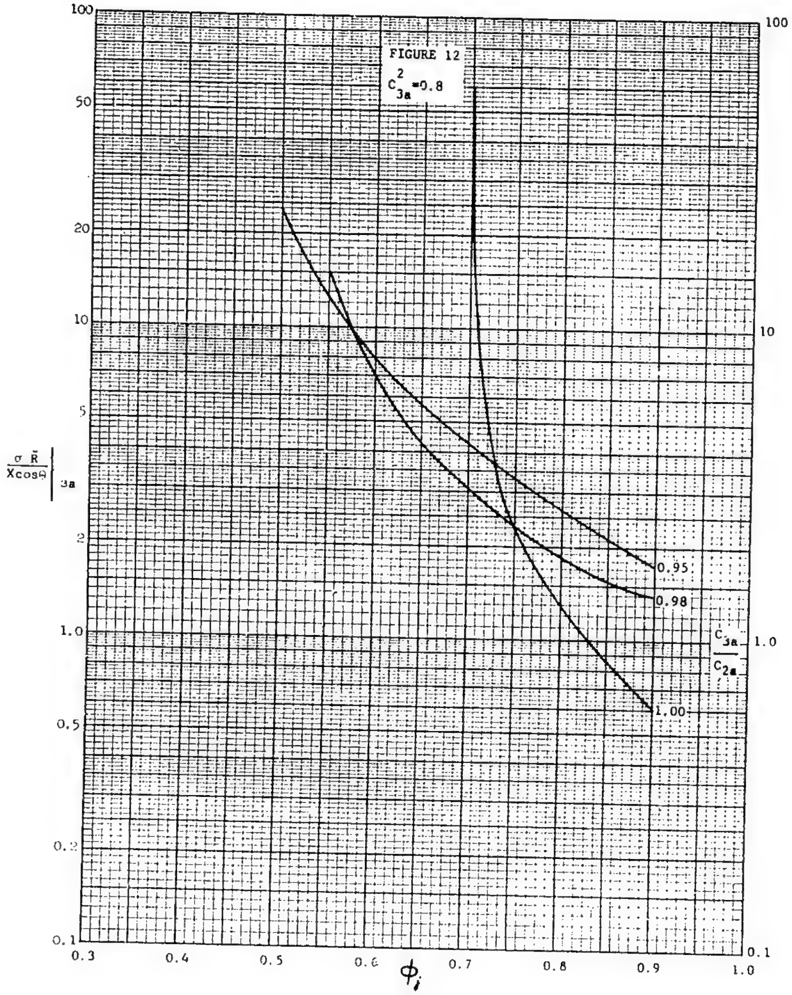
FIGURE 12
$C_{3a}^2 = 0.8$
$\left.\frac{\sigma \bar{R}}{X\cos\theta}\right|_{3a}$
ϕ_i
$\frac{C_{3a}}{C_{2a}}$
0.95
0.98
1.00

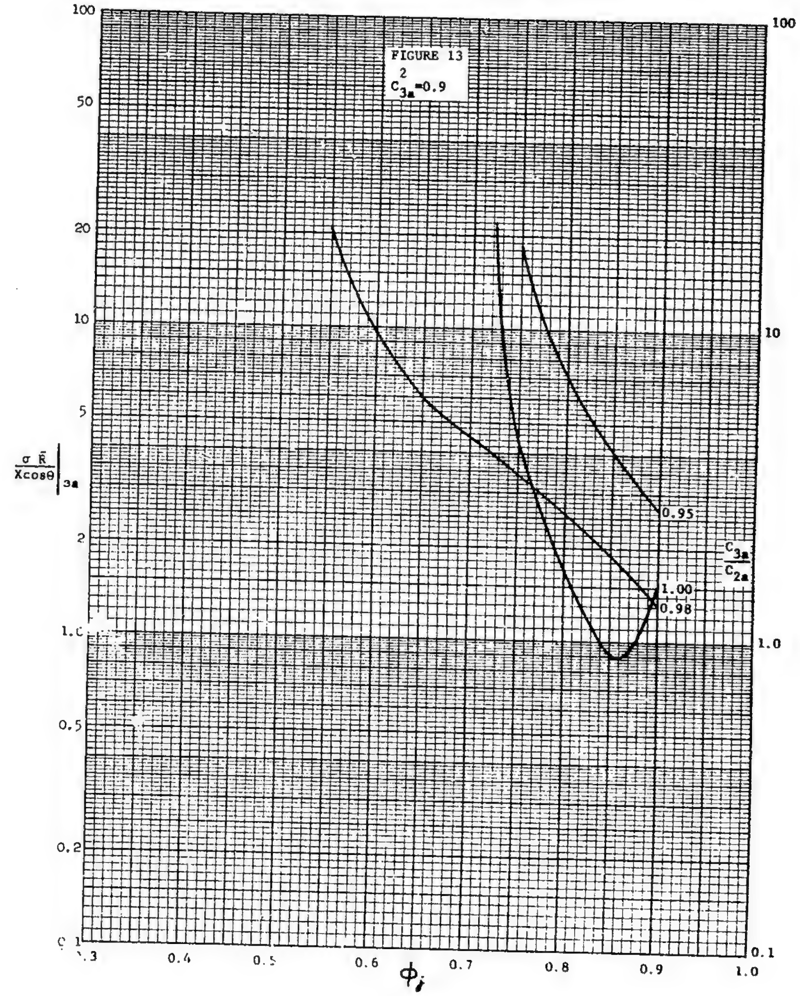
FIGURE 13
$C_{3a}^2 = 0.9$
$\left.\frac{\sigma \bar{R}}{X\cos\theta}\right|_{3a}$
ϕ_i
$\frac{C_{3a}}{C_{2a}}$
0.95
1.00
0.98

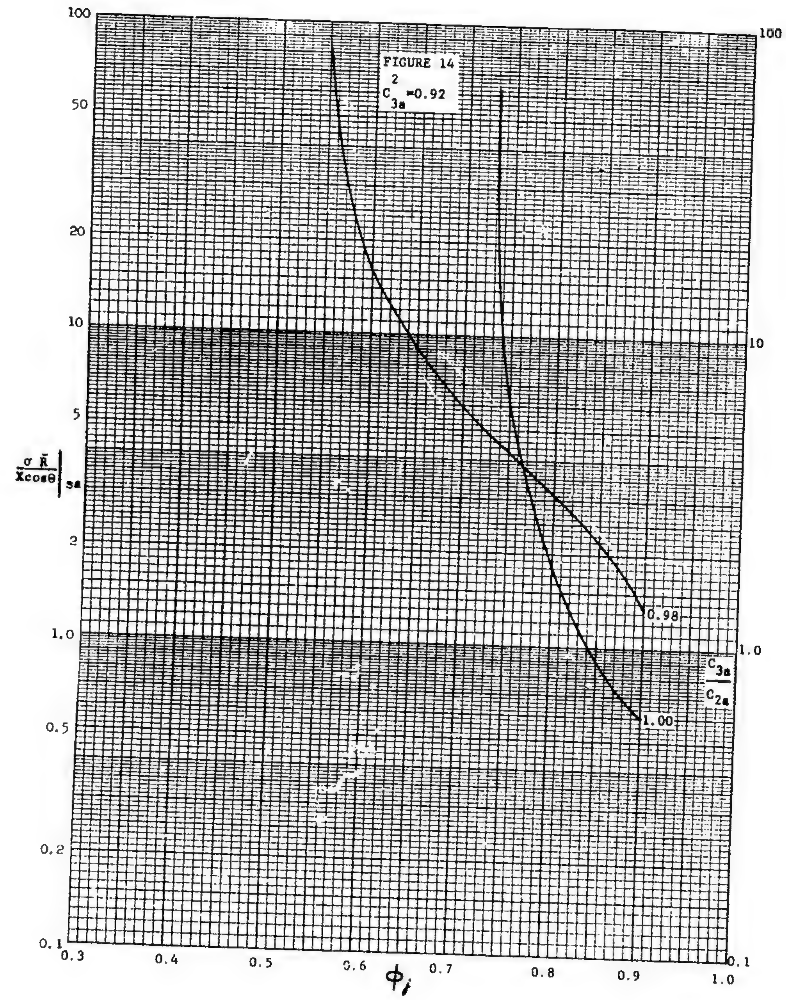
FIGURE 14
$C_{3a}^2 = 0.92$
$\frac{\sigma \bar{R}}{X\cos\theta}\Big|_{sa}$
$\frac{C_{3a}}{C_{2a}}$
0.98
1.00
ϕ_i
100
50
20
10
5
2
1.0
0.5
0.2
0.1
0.3
0.4
0.5
0.6
0.7
0.8
0.9
1.0

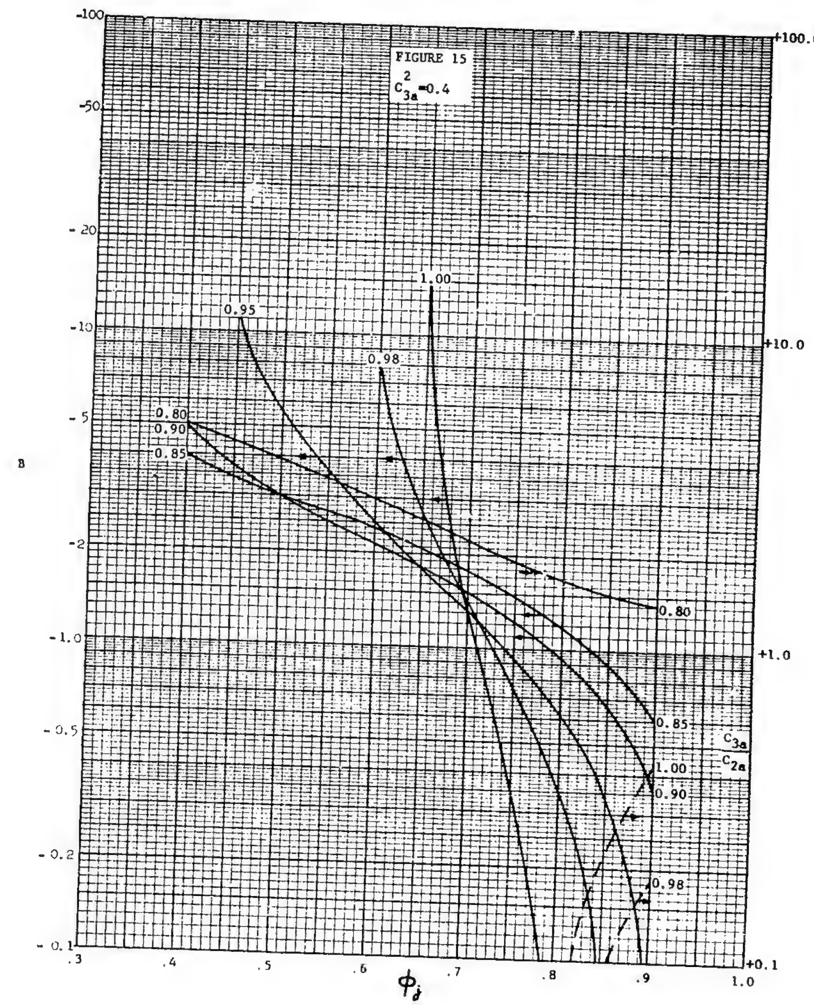
FIGURE 15
$C_{3a}^2 = 0.4$
B
$\frac{C_{3a}}{C_{2a}}$
1.00
0.95
0.98
0.80
0.90
0.85
ϕ_j
-100
-50
-20
-10
-5
-2
-1.0
-0.5
-0.2
-0.1
+100.0
+10.0
+1.0
+0.1
.3
.4
.5
.6
.7
.8
.9
1.0

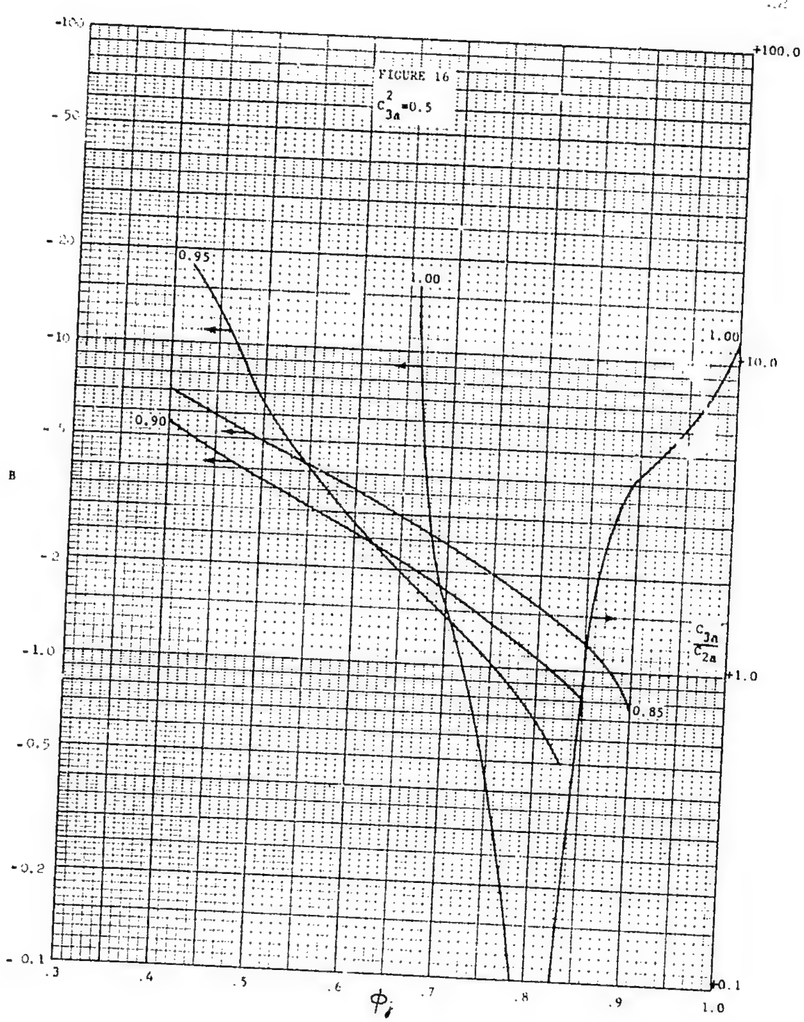
FIGURE 16
$C^2_{3a} = 0.5$
B
ϕ_i
$\frac{C_{3a}}{C_{2a}}$
0.95
0.90
1.00
0.85
-100
-50
-20
-10
-5
-2
-1.0
-0.5
-0.2
-0.1
+100.0
+10.0
+1.0
+0.1
.3
.4
.5
.6
.7
.8
.9
1.0

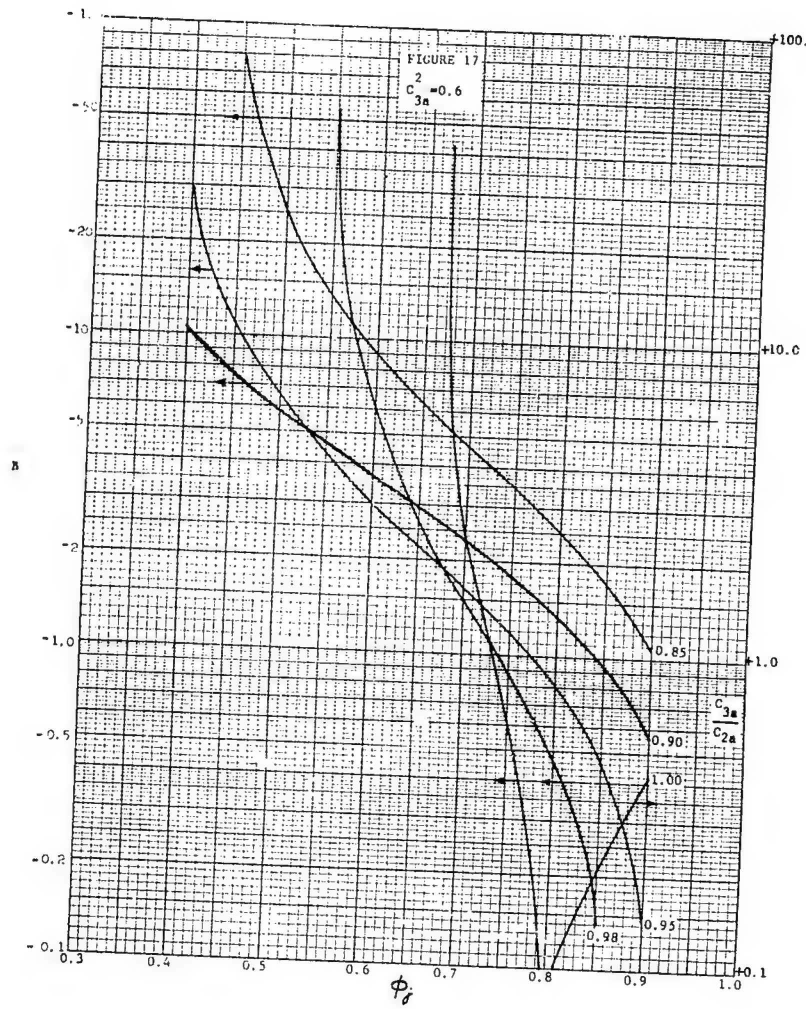
FIGURE 17
$C^2_{3a} = 0.6$
B
ϕ_i
$\frac{C_{3a}}{C_{2a}}$
0.85
0.90
1.00
0.95
0.98
-50
-20
-10
-5
-2
-1.0
-0.5
-0.2
-0.1
+100.0
+10.0
+1.0
+0.1
0.3
0.4
0.5
0.6
0.7
0.8
0.9
1.0

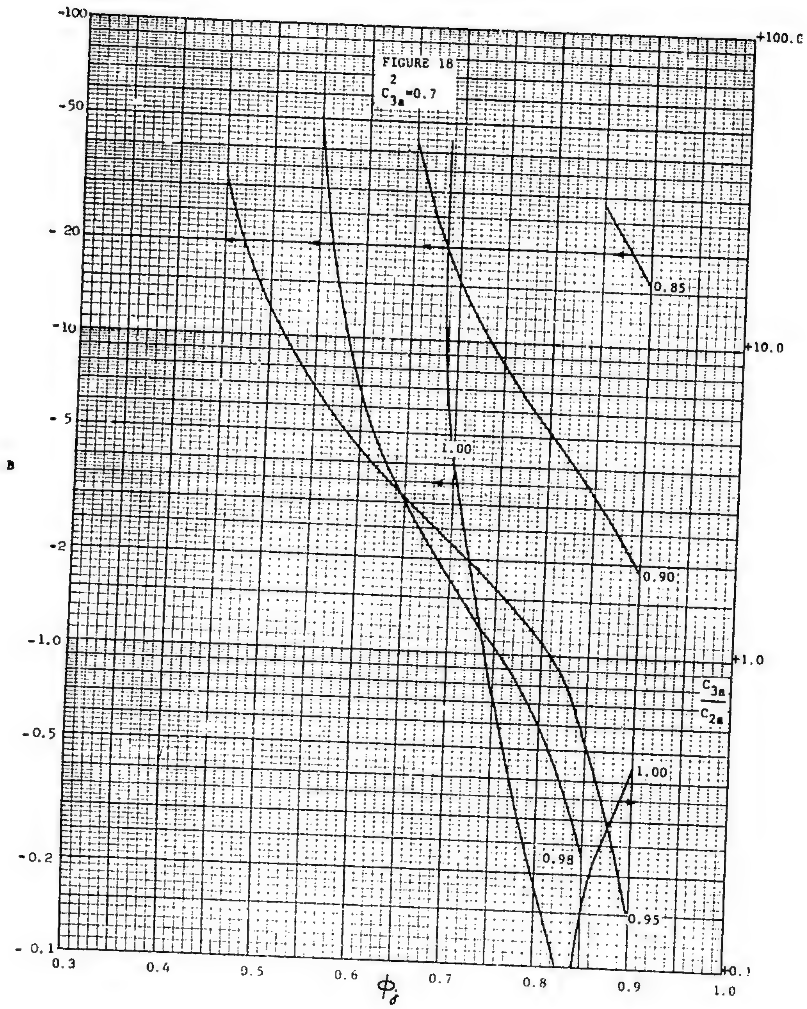
FIGURE 18
$C_{3a}^2 = 0.7$
0.85
0.90
1.00
0.98
0.95
1.00
$\frac{C_{3a}}{C_{2a}}$
B
ϕ_δ

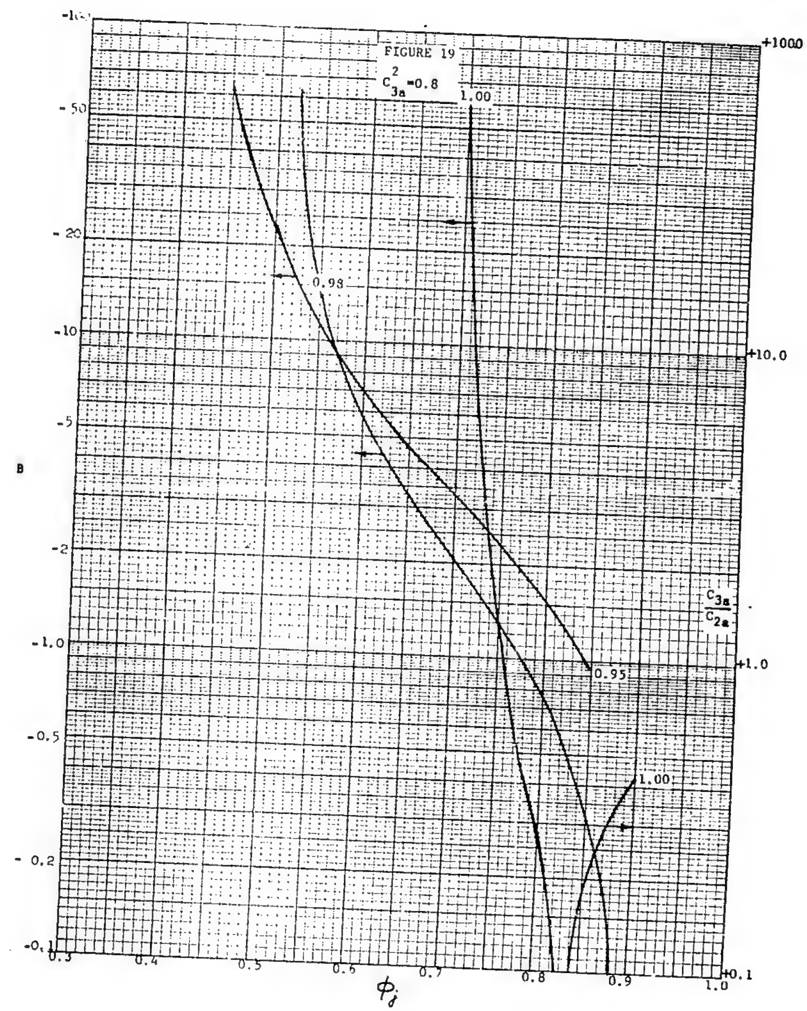
FIGURE 19
$C_{3a}^2 = 0.8$
1.00
0.98
0.95
1.00
$\frac{C_{3a}}{C_{2a}}$
B
ϕ_δ

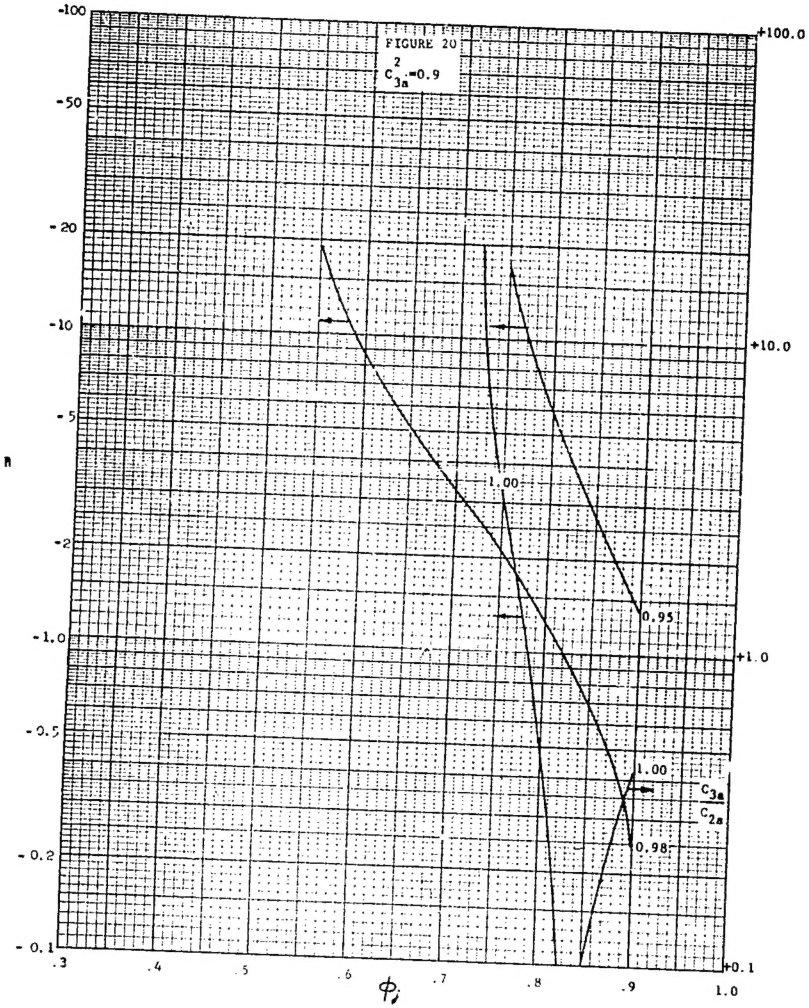
FIGURE 20
$C_{3a}^2 = 0.9$
-100
-50
-20
-10
-5
-2
-1.0
-0.5
-0.2
-0.1
+100.0
+10.0
+1.0
+0.1
.3
.4
.5
.6
.7
.8
.9
1.0
ϕ_i
1.00
0.95
1.00
0.98
$\frac{C_{3a}}{C_{2a}}$

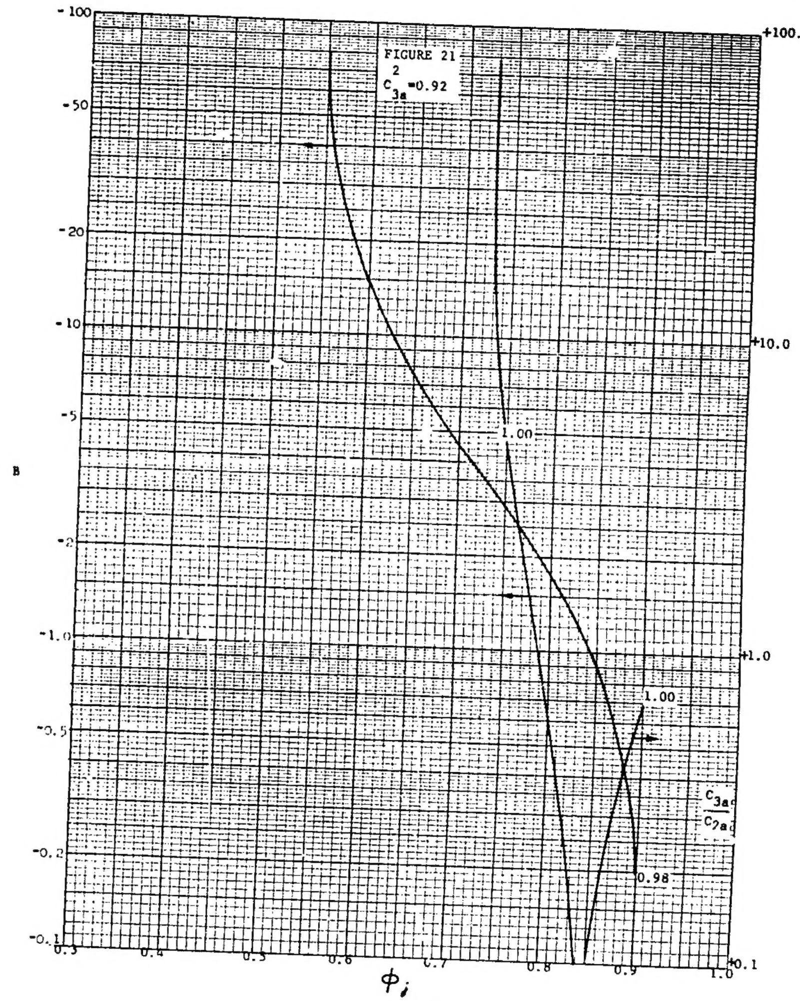
FIGURE 21
$C_{3a}^2 = 0.92$
-100
-50
-20
-10
-5
-2
-1.0
-0.5
-0.2
-0.1
+100.0
+10.0
+1.0
+0.1
0.3
0.4
0.5
0.6
0.7
0.8
0.9
1.0
ϕ_i
B
1.00
1.00
0.98

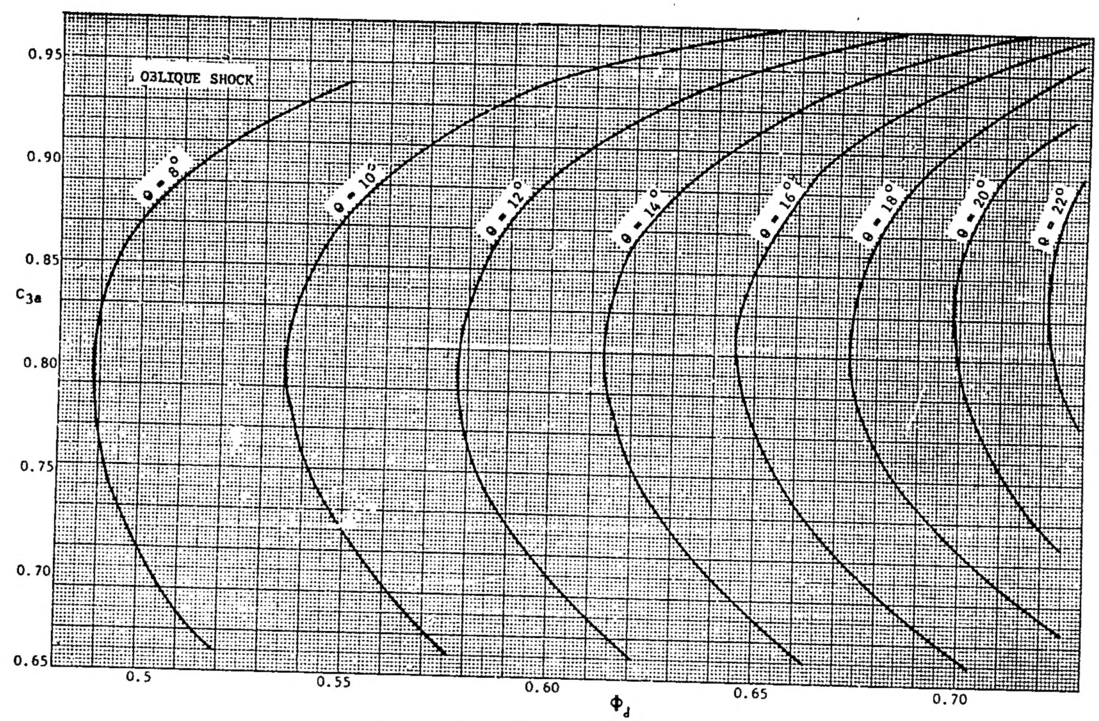

Fig. 22 C_3 vs. Φ_d for Various θ_{34}

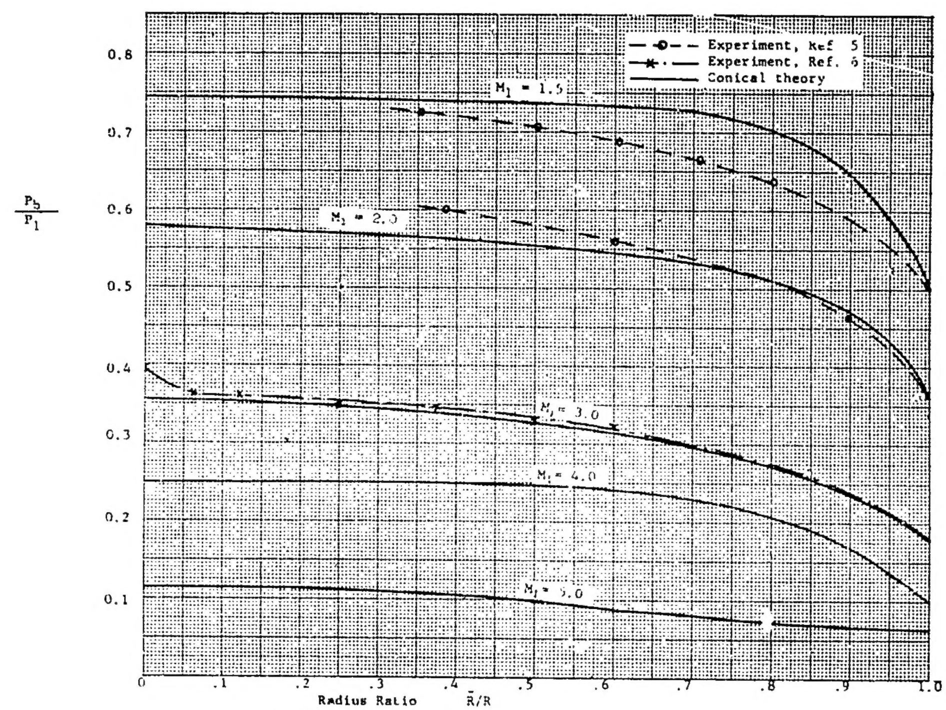

Fig. 23 Comparison of the Conical Flow Theory with Experiment for External Flow Past a Cylinder with Reduced Radius.

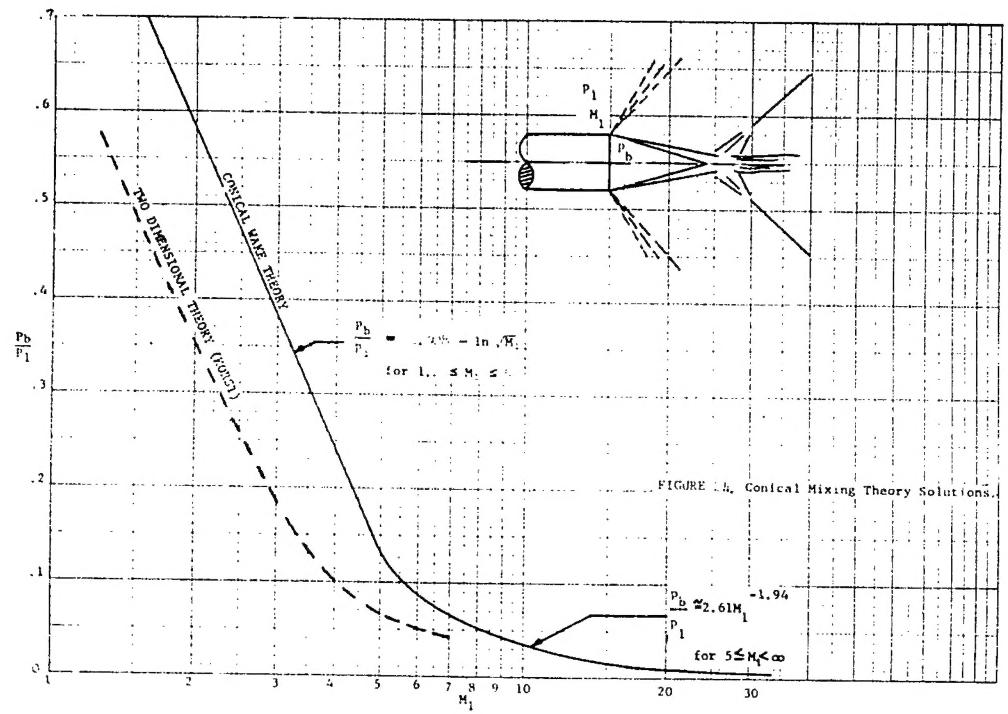

FIGURE 14. Conical Mixing Theory Solutions.

END